Ultrastructure and hemodynamics of microaneurysms in retinal vein occlusion examined by an offset pinhole adaptive optics scanning light ophthalmoscope

SHIN KADOMOTO, YUKI MURAOKA,* AKIHITO UJI, RYOSUKE TAMIYA, ⓘD SOTARO OOTO, TOMOAKI MURAKAMI, YASUYUKI ORITANI, KENTARO KAWAI, AND AKITAKA TSUJIKAWA

Department of Ophthalmology and Visual Sciences, Kyoto University Graduate School of Medicine, Kyoto, Japan
*muraoka@kuhp.kyoto-u.ac.jp

Abstract: Retinal microaneurysms (MAs) associated with retinal vein occlusions often cause macular edema due to vascular leakage from the MAs, which can lead to severe vision loss. However, studies using conventional imaging modalities have not shown a significant association between MAs and retinal functional changes. The recent technological advancements to the adaptive optics scanning light ophthalmoscope (AOSLO) have enabled real-time observation of the human retinal microvasculature. Additionally, offsetting the confocal aperture in the AOSLO enables the blocking of specular reflection from the inner retina and the enhancement of the image contrast of the retinal capillaries. This study investigated the ultrastructure and hemodynamics of MAs examined by structural images and perfusion maps of the offset pinhole AOSLO and evaluated their associations with vascular leakage on fluorescein angiography. Our results show the diverse configurations of the MAs, some of which are occasionally accompanied by a cap structure on the aneurysmal surface. Moreover, the morphological and hemodynamic changes were significantly associated with vascular leakage.

1. Introduction

Retinal vein occlusions (RVOs) are one of the most common retinal vascular diseases [1–3]. Occlusion of the retinal veins can upregulate vascular endothelial growth factor (VEGF) and cause vision-threatening macular edema (ME) [4]. The recent introduction of anti-VEGF therapies, which suppress upregulated VEGF and concomitant vascular leakage, has improved visual outcomes of eyes with RVO [5–8]. However, the recurrence of ME refractory to anti-VEGF therapies is common among RVO-patients [9]. Tsuboi et al reported that developments of retinal vascular remodeling, including retinal microaneurysms (MAs), might be involved in such refractory conditions [10]. We can suspect the presence of the MA from the findings of hyperreflective dots in the upper and/or lower borders of the inner nuclear layer on optical coherence tomography (OCT) B-scan or hyperreflective bulges originating from affected retinal capillaries on OCT angiography (OCTA) [9–11]. However, it might be quite difficult for the limited resolution power of these modalities to capture the essential features of the MAs associated with fluorescein leakage.

Adaptive optics (AO) is an approach that was originally developed for correcting an atmospheric fluctuation, which can obscure astronomical observations [12]. The AO scanning light ophthalmoscope (AOSLO) is an imaging device, the transverse resolution of which can reach 3 µm by correcting the aberration existing in the ocular surfaces [13–15]. Using the AO examinations for eyes with diabetic MAs, the hyperreflective wall structure [16], association

between intra-aneurysmal hemodynamics and clot location [17], and the three-dimensional structure [18] were demonstrated. Additionally, Chui et al recently reported that offsetting the confocal aperture in the AOSLO was useful for blocking the specular reflection from the inner retina and enhanced the image contrast of the retinal capillaries including diabetic MAs [19–21]. Thus, observations of retinal circulation using AOSLO mainly targeted healthy and diabetic vasculatures, and imaging of the MAs associated with RVO has received insufficient examination with the offset pinhole AOSLO approach.

In this study, to elucidate the morphologic and functional factors associated with retinal vascular leakage from RVO-MAs, we elaborately examined the macular MAs using FA and offset pinhole AOSLO.

2. Methods

2.1. Patients

This observational, cross-sectional case series study was approved by the Institutional Review Board of Kyoto University Graduate School of Medicine (Kyoto, Japan), and adhered to the tenets of the Declaration of Helsinki. Written informed consent was obtained from each subject before any study procedures or examinations were conducted.

We enrolled patients with unilateral branch RVO accompanying MAs in the macular area, examined at the Department of Ophthalmology of Kyoto University Hospital between April 2018 and January 2020. We excluded eyes with co-existing ocular disease (diabetic retinopathy, hypertensive retinopathy, retinal arterial occlusion, retinal macroaneurysm, glaucoma, retinitis pigmentosa, or age-related macular degeneration) or the presence of any of following: keratoconus, high myopia (more severe than -6 diopters), or high astigmatism (more severe than ±3 diopters). Additionally, we excluded eyes with poor-quality AOSLO images when the AO systems could not appropriately work due to eye movement or strong media opacities.

All eyes were diagnosed as acute branch RVO with ME at the initial visit. Foveal cystoid spaces and/or serous retinal detachment was observed for all included eyes at the time of the initial visit. As treatment for ME, each eye initially received monthly intravitreal ranibizumab (0.5 mg/0.05 mL) injection for three months. An additional injection was administered thereafter, if ME and/or serous retinal detachment were evident in the fovea on optical coherence tomography (OCT) sections. These eyes received no other treatment, such as grid laser photocoagulation, steroid therapy, surgical intervention, or anti-VEGF agents other than ranibizumab, for ME. Each eye was examined for 12 months after the initial visit. At each visit, all patients underwent routine ophthalmic examinations, including the measurement of best-corrected visual acuity (VA), using a Landolt chart, intraocular pressure, slit-lamp biomicroscopy, and spectral domain OCT (Spectralis HRA + OCT, Heidelberg Engineering, Heidelberg, Germany). Foveal thickness was measured using macular volume scans obtained via the OCT. A whole-retinal thickness map centered on the fovea was created. Foveal thickness was defined as the average value calculated from the retinal thickness within the central subfield of the Early Treatment Diabetic Retinopathy Study grid.

At more than one year after the initial ranibizumab injection, each patient underwent FA (Spectralis HRA + OCT, Heidelberg Engineering, Inc., Heidelberg, Germany), prototype offset pinhole AOSLO (Canon, Inc., Tokyo, Japan), and routine examinations on the same day to examine morphologic and functional changes in the MAs and their associations with persistent or refractory ME. The examinations revealed no retinal hemorrhage within the fields of views. The ME was also substantially absorbed. Even if the ME was present, its severity was insufficient to affect image quality. For patients requiring additional anti-VEGF treatment, the FA and the offset pinhole AOSLO were performed before the treatment.

2.2. Examinations with fluorescein angiography

Fluorescein angiography images centered on the fovea had been obtained for about 10 minutes after an intravenous bolus infusion of fluorescein dye. The MAs were detected as hyperfluorescent dots in the early phase obtained at around 1 min after dye injection. In this study, the MAs located within 15 degrees from the center of the fovea were evaluated. Two fully trained retina specialists (S.K. and Y.M.) judged the presence or absence of fluorescence leakage by comparing FA images obtained at 1 min (early phase) with those obtained at 5 min (late phase) (Fig. 1). We defined fluorescein leakage as any increased intensity over the choroidal background, within the retina, but outside the retinal vasculature (Fig. 1). Additionally, when the presence of an MA was within a roughly circular area of leakage, and when the intensity of leakage decreased as the distance from the MA increased, we considered that the MA was the source of leakage (Fig. 1). In the evaluations of the leakage, we defined no or questionable leakage as the absence of leakage and definite leakage as the presence of leakage based on the evaluation methods of previous reports (Fig. 1) [22, 23].
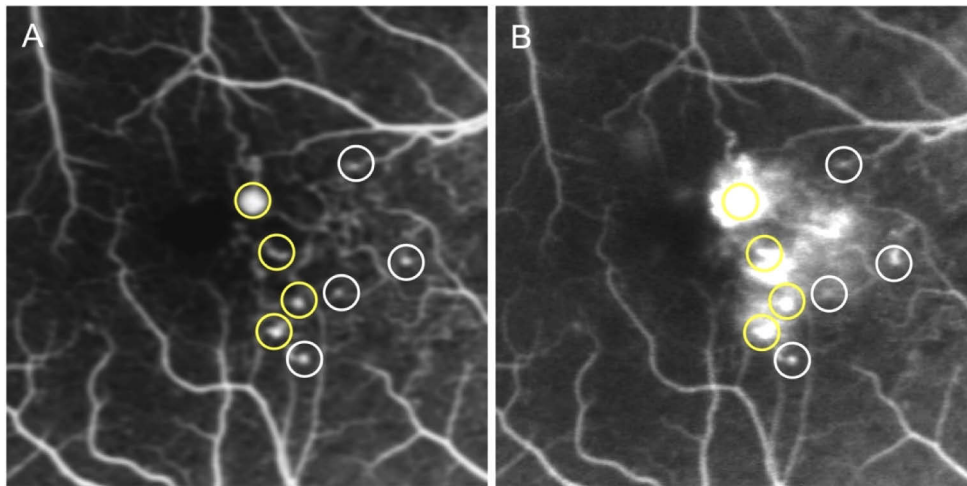

Fig. 1. Detection of microaneurysms (MAs) and the evaluation of the associated-dye leakage using fluorescein angiography (FA). FA images obtained at the early (**A**) and late (**B**) phases. The MAs are shown as hyperfluorescent dots in the early phase. Fluorescein leakage is defined as any increased intensity over the choroidal background, within the retina, but outside the retinal vasculature. Yellow and white circles indicate MAs with and without significant leakage, respectively.

2.3. Offset pinhole AOSLO imaging

We imaged the MAs and the associated vessels, which were located 15° from the center of the fovea, fitted into the viewing angles, using a prototype offset pinhole AOSLO system (Canon, Inc., Tokyo, Japan), which could achieve a high wavefront correction efficiency with a deformable mirror (Fig. 2).

The imaging wavelength was 795 ± 8.5 nm, and the beam diameter was 6.7 mm at the pupil of the eye, producing a diffraction-limited transverse resolution of approximately 3 μm within the retina. The system enables the configuration of confocal and offset pinhole imaging simultaneously. In this study, the confocal pinhole size was 48 μm, which equaled the airy disk diameter (1 ADD) of the system. The pinhole size of the offset pinhole imaging was 344 μm (7 ADD). The pinholes were offset by 180 μm (3.75 ADD) in opposite directions in the plane horizontal to the retina. In the retinal space, the confocal pinhole size, the pinhole size of the
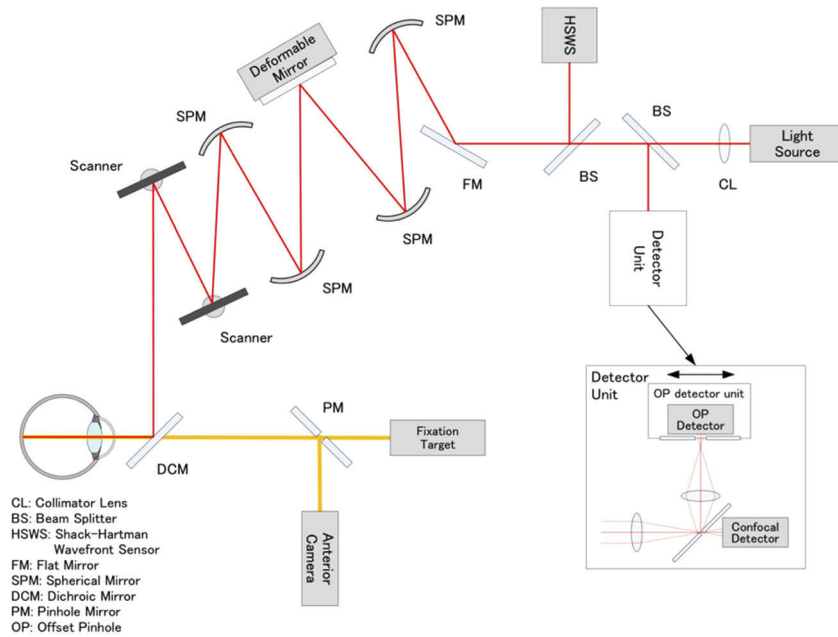
Fig. 2. Schematic representation of the optical structure of adaptive optics scanning light ophthalmoscope. Collimated near-infrared light from the light source propagates through the spherical mirrors, beam splitters, and dichroic mirror to the subject's eye. Two scanners are used to scan the imaging light two-dimensionally on the retina. Ninety-seven-actuator deformable mirror is used to compensate the eye's aberration, which is measured by the Shack-Hartman wavefront sensor. The confocal light is detected by the confocal detector of the detector unit through the pinhole, and the light outside the pinhole is reflected to the offset pinhole detector. The light for the fixation target and the anterior camera are combined by the dichroic mirror. The pinhole size of the confocal imaging was 48 μm, which equaled the airy disk diameter (1 ADD) of the system. The pinhole size of the offset pinhole imaging was 344 μm (7 ADD). The pinholes were offset by 180 μm (3.75 ADD) in opposite directions in the plane horizontal to the retina.

offset pinhole imaging, and offset distance of pinholes were 4.92 μm, 34.45 μm, and 18.46 μm, respectively. A 1 ADD pinhole mirror sent the central portion of the point spread function to a first avalanche photodiode (Channel 1) for confocal imaging, whereas the light outside this area (within an ~7 ADD circular aperture) was split and sent to two additional avalanche photodiodes (Channels 2 and 3). One offset pinhole image from one of the two additional avalanche photodiodes (Channel 3) was used in this study. The field of view of offset pinhole AOSLO was 1.2 × 1.2 degree (360 × 360 μm) at the retina and was sampled at 448 × 448 pixels. Each AOSLO video was acquired for 3 seconds per scan area at 30 frames per second (~89 frames per sequence). The raw AOSLO data were corrected for scanning distortions and were stabilized to correct for eye motion by using a customized software (Canon, Inc.). The registration technique of the software was based on scan line warping, and the fixed reference frame (the first of 89 frames) was used for image warping [24].

Each offset-pinhole AOSLO image with high signal-to-noise ratio was generated by averaging 20 to 89 frames in the registered sequence, which resulted in the offset pinhole AOSLO structural image. Next, using the previously described standard deviation method [24–26], we sequentially registered AOSLO images (89 frames per second) and created perfusion maps (motion contrast images) representing the variance of signal intensity in blood cells (mainly erythrocytes). When

the movement of the blood cells was more rapid, the brightness of the vessels or MAs was higher on the AOSLO perfusion map.

Before AOSLO imaging, the pupils of all the examined eyes were fully dilated with tropicamide (0.5%) and phenylephrine hydrochloride (0.5%) drops (Mydrin-P ophthalmic solution, Santen Pharmaceutical Co., Ltd, Osaka, Japan).

2.4. MAs classification

Using the structural images of offset pinhole AOSLO, two fully trained examiners (S.K. and Y.M.) independently classified all the 71 MAs morphologically, based on previous pathologic reports [27, 28], or on the AOSLO examination for the human diseased retinas [29]. If the graders had discrepancies regarding a particular case, they had an open discussion to produce a single determination.

In this study, we first divided all the MAs into two groups: the smaller focal bulge and the larger non-focal bulge. The latter group was subcategorized into saccular, fusiform, and mixed types (Fig. 3, see Visualization 1, Visualization 2, Visualization 3, and Visualization 4). The characteristics of the morphological types are as follows:

1. Focal bulge group: relatively smaller, with the configuration slightly protruding from either side of the associated vessel walls (Fig. 3(A), see Visualization 1).

2. Non-focal bulge group: MAs other than the focal bulge group; relatively bigger.

a) Saccular type:

   The MAs dilating asymmetrically to the long axis of the associated vessels. Differing from the focal bulge MAs, their main body was much bigger than the root part just branching from the associated vessels (Fig. 3(C), see Visualization 2).

b) Fusiform type:

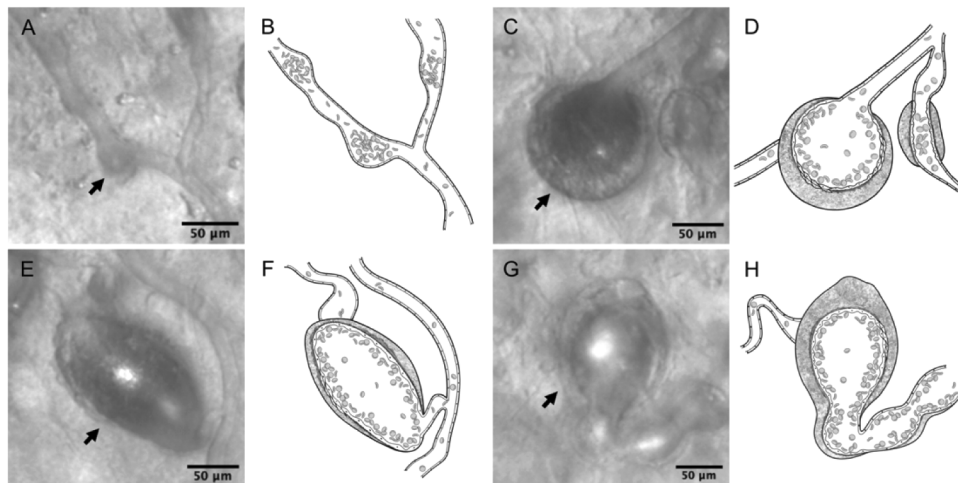
Fig. 3. Morphological classifications of microaneurysms (MAs) associated with retinal vein occlusion. (**A-B**) Focal bulge type (arrow). (**C-H**) Non-focal bulge type, which are larger than non-focal bulge MAs. (**C-D**) Saccular type (arrow). (**E-F**) Fusiform type (arrow). (**G-H**) Mixed type (arrow). (**B,D,F,H**) Illustrations of each Figure of first and third column, respectively.

The MAs dilating symmetrically to the long axis of the associated vessels, which was different from the hemi-side dilation of the focal bulge MAs and the asymmetric dilation of the saccular type (Fig. 3(E), see Visualization 3).

c) Mixed type:

The MAs having characteristics of both the saccular and fusiform types (Fig. 3(G), see Visualization 4).

2.5. Quantitative evaluations of morphology and hemodynamics of the MAs and associated vessels

The AOSLO imaging showed that some MAs had a wall-like and highly reflective structure around the surfaces, which we termed cap structure (Fig. 4(A)). We measured the mean caliber of the associated vessels at sites 10 μm proximal and distal to the MA edge, the whole MA area (including the area of aneurysmal cap, if existing), lumen area, and the area size of the cap structure on the AOSLO structural image by using ImageJ version 1.52b (National Institutes of Health, Bethesda, MD; https://imagej.nih.gov/ij/index.html) (Fig. 4(B)). Each parameter was additionally corrected using the modified Littmann formula (Bennett procedure) [30] to allow for axial length-related magnification. Determinations of the outlines of MAs and associated vessels were partially based on subjective judgments. Therefore, to confirm the validity of quantitative parameters regarding the MAs, two trained examiners (S.K. and R.T.) independently measured those parameters by manually delineating the AOSLO images, and then calculated the intraclass correlation coefficients (ICCs).

To evaluate blood cell motions (BCM) within the MA, we set an index, which was defined as the ratio of mean gray value within the MA to that within associated vessels on an AOSLO perfusion map (Fig. 4(D)). A BCM index of >1 indicates greater hemodynamic activity (variances in the pixel intensities) of the intra-aneurysmal blood cells compared to those of the associated vessel.

2.6. Statistical analyses

We performed statistical analysis using JMP 14 (SAS Institute Inc., Cary, NC, USA), presenting all values as mean ± standard deviation. Comparisons between the two groups were performed using the unpaired t-test and bivariate relationships were analyzed via Pearson's correlational coefficient. We used the chi-square test to compare categorical variables. We considered P values less than 0.05 to be statistically significant.
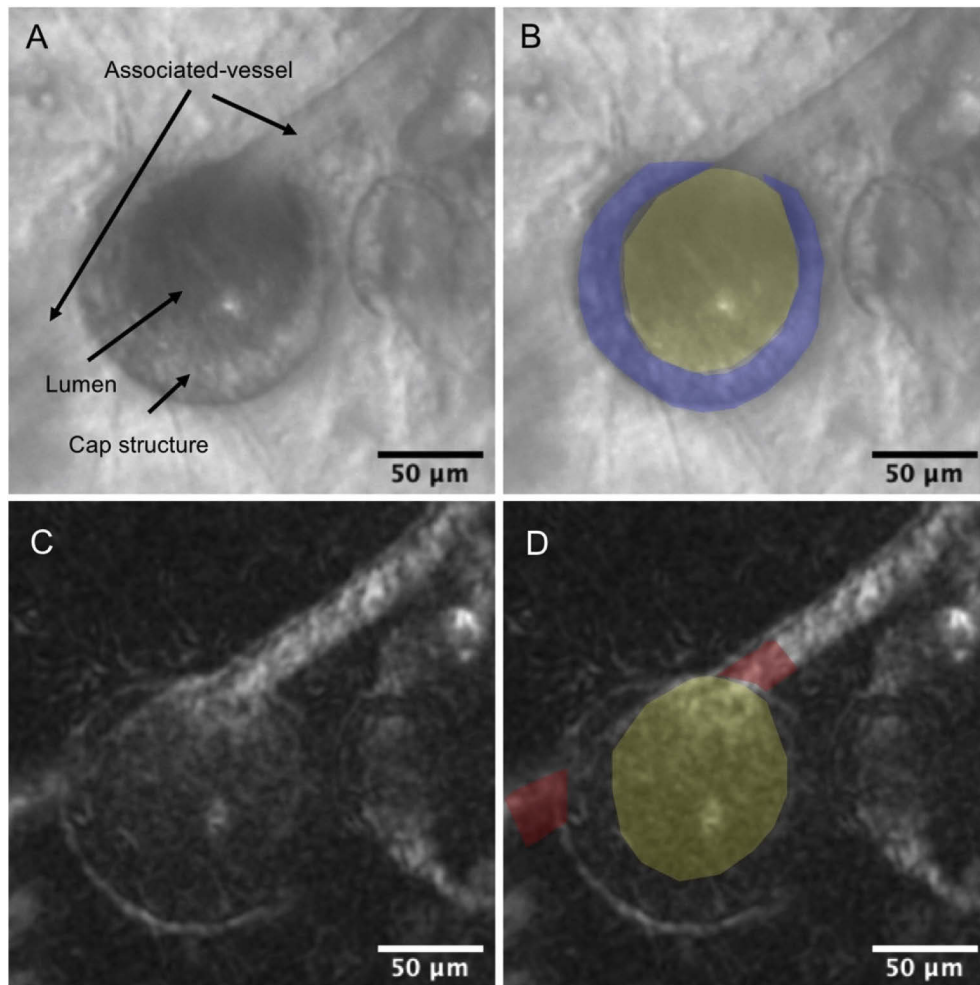
Fig. 4. Structural and hemodynamic adaptive optics scanning light ophthalmoscope (AOSLO) images of the microaneurysms (MAs) associated with retinal vein occlusion. (**A-B**) Microstructures of MA on offset pinhole AOSLO. The MA has the influx and efflux capillary (associated vessel) and crescent-shaped cap structure. The boundaries of the cap structure and the MA lumen are indicated in blue and yellow, respectively. (**C-D**) Intra-aneurysmal perfusion map on offset pinhole AOSLO. Brighter areas represent greater hemodynamic activity on the AOSLO perfusion map. The blood cell motion in MA is defined as the ratio of the mean gray value within the MA lumen (yellow) to that within the associated vessel (red).

3. Results

3.1. Patient background

Table 1 shows the characteristics of the included patients with unilateral branch RVO (9 men, 5 women; mean age 66.8 ± 6.8 years). At the initial visit, the logMAR VA was 0.26 ± 0.23, and foveal thickness was 585.2 ± 147.2 μm. At AOSLO and FA examinations, which were 25.4 ± 9.5 months from the onset, the logMAR VA improved to 0.02 ± 0.14, and foveal thickness decreased to 333.7 ± 68.9 μm. The foveal thickness significantly decreased compared to that at the initial visit ($P < 0.001$). However, mild retinal thickening remained at the macular area.

Table 1. Characteristics of patients with retinal vein occlusion[a]

Number of patients included (men/women)	9/5
Age (y)	66.8 ± 6.8
Systemic Hypertension, n	6
At initial visit	
Mean logMAR visual acuity	0.26 ± 0.23
Mean foveal thickness (μm)	585.2 ± 147.2
At AOSLO examination	
Mean time from onset to AOSLO examination (month)	25.4 ± 9.5
Mean logMAR visual acuity	0.02 ± 0.14
Mean foveal thickness (μm)	333.7 ± 68.9
Number of ranibizumab injections required	5.3 ± 4.1
Number of microaneurysms per eye, (range, n)	2—18
Total number of microaneurysms examined, n	71

[a]AOSLO = adaptive optics scanning light ophthalmoscope; logMAR = logarithm of the minimal angle of resolution. Data are mean ± standard deviation unless otherwise indicated.

3.2. Morphological classifications of the RVO-MAs examined by AOSLO

High transverse resolution, and high contrast of the offset pinhole AOSLO enabled visualization of the ultrastructure affected by RVO.

Out of all the 71 MAs examined, the focal bulge group was 19.7%, and non-focal bulge group was 80.3%. Out of the non-focal bulge MAs, saccular, fusiform and mixed types were 49.3%, 19.7%, and 11.3%, respectively (Table 2)

Table 2. Morphological classifications of retinal vein occlusion associated-microaneurysms and other parameters examined by adaptive optics scanning light ophthalmoscope[a]

		Morphological classification				
	Focal bulge	Non-focal bulge				*P* value*
		Total	Saccular	Fusiform	Mixed	
Number	14 (19.7%)	57 (80.3%)	35 (49.3%)	14 (19.7%)	8 (11.3%)	N.A.
Caliber of associated vessel (μm)	12.0 ± 3.0	14.4 ± 4.7	13.6 ± 5.3	14.9 ± 5.1	16.7 ± 4.2	0.057
Whole area (μm^2)	974.9 ± 879.1	2888.4 ± 2924.4	2375.6 ± 2394.0	2819.6 ± 2762.3	2847.3 ± 1753.9	0.019
Lumen area (μm^2)	950.4 ± 888.2	1834.4 ± 1813.6	1516.2 ± 1315.7	2046.3 ± 2294.1	1575.3 ± 1095.0	0.082
Presence of cap structure (Ratio, %)	1/14 (7.1%)	37/57 (64.9%)	21/35 (60.0%)	9/14 (64.3%)	7/8 (87.5%)	<0.001
Intra-aneurysmal BCM	1.38 ± 0.25	1.16 ± 0.31	1.15 ± 0.35	1.11 ± 0.17	1.26 ± 0.33	0.018

[a]BCM = blood cell motion. *Comparisons between focal bulge and non-focal bulge using unpaired *t*-test.

3.3. Morphologic and hemodynamic changes in the RVO-MAs examined by AOSLO

The intra-evaluator ICCs were more than 0.940 for each AOSLO parameter of the affected retinal vasculatures, which were highly reproducible.

Table 2 shows morphologic and functional changes in the MAs examined. The whole areas of the MAs were 974.9 ± 879.1 μm^2 in the focal bulge group and 1834.4 ± 1813.6 μm^2 in the

non-focal bulge group (*P*=0.019). However, the lumen areas of the MAs were not significantly different between the two groups (Table 2).

The offset pinhole AOSLO occasionally detected highly reflective parts on the aneurysmal surface, which we termed as "cap" structure in this study (Fig. 4, see Visualization 2, Visualization 3, Visualization 4, Visualization 5). The detection rate of the cap was 7.1% in the focal bulge group (1/14) and 64.9% in the non-focal bulge group (37/57) (*P*<0.001).

Additionally, the AOSLO videos enabled to track time-lapse motions of the blood cells (mainly erythrocytes) in both the associated vessels and the MAs. The BCM were relatively constant in the associated vessels (see Visualization 1, Visualization 2, Visualization 3, Visualization 4, and Visualization 5).

The BCM in the MAs were diverse in the various morphological types. In the focal bulge group, the BCM were uniformly more rapid and turbulent (see Visualization 1). The BCM index was 1.38 ± 0.25 in the focal bulge group and 1.16 ± 0.31 in the non-focal bulge group (*P*=0.018; Table 2).

In contrast, the BCM of the non-focal bulge MAs were more complicated. Especially in the MA accompanying the cap structure, BCM were uneven in identical MAs, and more stagnant near the cap (see Visualization 2, Visualization 3, Visualization 4, Visualization 5). In the non-focal bulge MAs, the BCM index was 1.15 ± 0.24 in the MAs with the cap and 1.34 ± 0.29 in those without the cap (*P*<0.001; Table 3).

Table 3. Associations between the cap structure and other parameters related to retinal vein occlusion-associated microaneurysms using adaptive optics scanning light ophthalmoscope examinations[a]

	Cap structure				
	Area size		Present (n=38)	Absent (n=33)	*P* value*
	R	*P* value			
Morphology (focal bulge/non-focal bulge; n)	N.A.		1/37	13/20	<0.001
Caliber of associated vessel (μm)	0.102	0.057	14.6 ± 5.2	12.9 ± 3.4	0.142
Whole area ($μm^2$)	0.811	<0.001	2921 ± 2791	1435 ± 841.3	0.005
Lumen area ($μm^2$)	0.539	<0.001	1570 ± 1914	1435 ± 841.3	0.670
Intra-aneurysmal BCM	-0.564	<0.001	1.15 ± 0.24	1.34 ± 0.29	<0.001

[a]BCM = blood cell motion; *Comparison between perianeurysmal cap present group and absent group using unpaired *t*-test; The presence of perianeurysmal cap between each morphology, and the presence of fluorescence leakage were evaluated with the chi-square test.

3.4. Associations between fluorescein leakage and AOSLO parameters in RVO-MAs

On FA, we detected significant fluorescein leakage in 51 of the 71 MAs (71.8%). Table 3 shows associations between fluorescein leakage and the AOSLO parameters of the examined eyes.

The calibers of the associated vessels and the whole and lumen areas of the MAs were not significantly different between the MAs with and without fluorescein leakage. However, the morphology of the non-focal bulge, the presence and larger size of the cap structure and lower BCM were significantly associated with the presence of retinal vascular leakage (*P*<0.001, *P* = 0.018, *P*=0.007, *P* = 0.021, respectively; Table 4; Fig. 5, see Visualization 5).
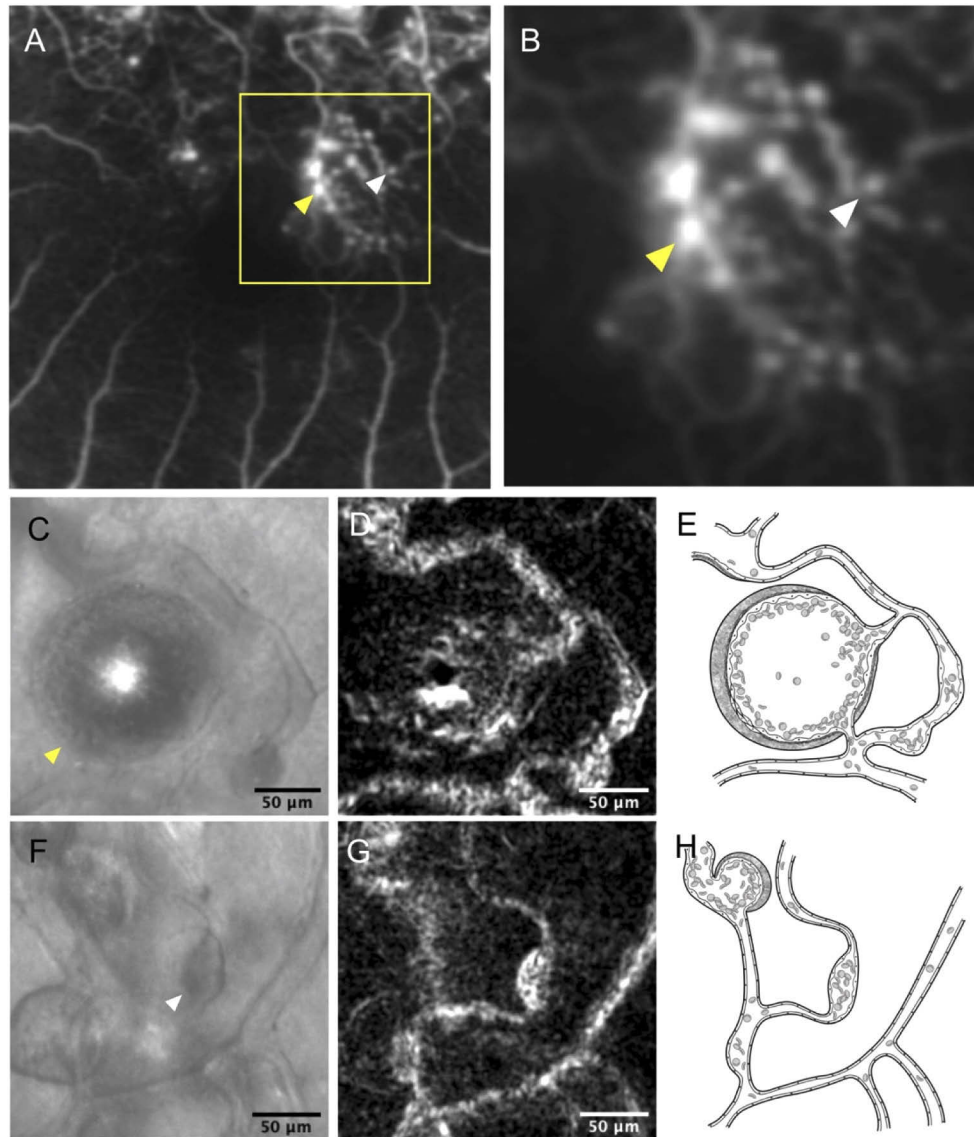
Fig. 5. Retinal vein occlusion associated-microaneurysms (MAs) with or without fluorescein leakage. (**A**) Fluorescein angiogram at the late phase within 15 degrees from the center of the fovea. Microaneurysms with fluorescein leakage (yellow arrowhead), and those without (white arrowhead), are indicated. (**B**) The magnified image of the yellow square area. (**C-E**) The MA with significant fluorescein leakage. The fluorescein angiogram at the late phase shows fluorescein leakage from the MA (yellow arrowhead). (**C**) The saccular MA visualized by offset pinhole adaptive optics scanning light ophthalmoscope (AOSLO). The saccular MA has the cap structure, and the whole area including the cap is 13590.1 μm^2. (**D**) The AOSLO perfusion map of the saccular MA. The brightness of the MA lumen is lower than that of the associated vessel. The value of blood cell motions (BCM) within the MA are 0.63. The brightness of the MA is heterogeneous on the AOSLO perfusion map, the center of which is higher than that of an area adjacent to the inner wall of the MA. (**E**) Illustration of the MA in Fig. 5 C. (**F-H**) The MA without significant fluorescein leakage (white arrowhead). (**F**) The focal bulge MA visualized by offset pinhole AOSLO image (arrowhead). The focal bulge MA does not accompany cap structure, and the whole area of the MA is 760.5 μm^2. (**G**) The AOSLO perfusion map of the focal bulge MA. The brightness of the MA lumen is higher than that of the associated vessel. The value of the BCM are 1.41. (**H**) Illustration of the MA in Fig. 5 F.

Table 4. Associations between fluorescein leakage and other parameters related to retinal vein occlusion-associated microaneurysms using adaptive optics scanning light ophthalmoscope examinations[a]

	Fluorescein leakage		*P* value*
	Present n=51	Absent n=20	
FB/non-FB (saccular/fusiform/mixed)	4/47 (29/11/7)	10/10 (6/3/1)	<0.001
Caliber of associated vessel (μm)	14.0 ± 4.7	13.1 ± 3.9	0.553
Whole area (μm^2)	2765 ± 2670	1858 ± 2905	0.215
Lumen area (μm^2)	1754 ± 1703	1418 ± 1704	0.460
Intra-aneurysmal blood cell motion	1.15 ± 0.31	1.33 ± 0.28	0.021
Presence of cap structure (n, %)	32 (62.8%)	6 (30.0%)	0.018
Size of cap structure (μm^2)	1564 ± 1518	581.3 ± 287.9	0.007

[a]FB = focal bulge; *Comparison between fluorescence leakage present group and absent group using un-paired *t*-test. The presence of fluorescence leakage between FB and non-FB, and the presence of aneurysmal cap were evaluated with the chi-square test.

4. Discussion

In the current study, we used a prototype system of the offset pinhole AOSLO, and successfully obtained high-resolution and high-contrast direct images of the affected retinal vasculatures of eyes with RVO. Using the structural images of the offset pinhole AOSLO, we qualitatively divided the configurations of the MAs into two groups: focal bulge (20%) and non-focal bulge (80%) (Table 2). Out of the non-focal bulge MAs, the saccular type, fusiform type, and mixed type accounted for approximately 50%, 20%, and 10%, respectively (Table 2). The characteristic feature of the focal bulge MAs was the small protrusion from the hemi-side of the associated vessel walls (Fig. 2(A)). The mean sizes of the whole and lumen areas were significantly smaller than those of the non-focal bulge MAs (Table 2). Out of the non-focal bulge group, the fusiform MAs had symmetric protrusions from both-sides of the vessel walls, which were different from the focal bulge MAs (Fig. 2(E)). The asymmetric dilation of saccular MAs might be similar to the hemi-side dilation of the focal bulge MAs (Fig. 2 C). However, the main body of the saccular MAs was much bigger than the root part originating from the associated vessels, which was quite different from the small protrusion of the focal bulge MAs. We therefore speculated that non-focal bulge MAs (fusiform and saccular MAs) might be more mature and severe phenotypes than the focal bulge MAs.

The offset pinhole AOSLO occasionally detected a highly reflective cap structure on the aneurysmal surface (Fig. 2(C), see Visualization 2). The detection rate was much higher in the non-focal bulge MAs than in the focal bulge MAs (Table 2). On AOSLO, the cap was crescent-shaped; however, the reflectivity within the cap was occasionally heterogeneous (Fig. 4). A previous report using electron microscopy showed that diabetic mature MAs had vessel walls composed of thickened basal membrane and damaged endothelial cells, while the immature MAs did not have such thickened walls [28]. The cap structure, as commonly observed in the non-focal bulge MAs, were consistent in the walls of the mature MAs on electron microscopic examination. Endothelial cells of the retinal vessels physiologically emit various growth factors [31] and mediate vascular tone or maintain the homeostasis of the vessel walls [32]. However, in pathologic conditions including RVO, the abnormal shear stress would induce circumferential and penetrated proliferations of the endothelial cells in association with the upregulations of the growth factors [33, 34] and accelerate remodeling of the affected vessel walls [35]. In diabetic retinopathy, the wall of the saccular MAs was stained with von Willebrand factor, which is a marker of the endothelial cells, activated by cell damage [27]. This immunohistological finding might also suggest possible severe endothelial damage of the non-focal bulge MAs in this study.

Using confocal AOSLO, Lammer et al. recently reported the presence of hyperreflective walls in diabetic MAs and its association with larger MA sizes [16]. Despite being derived from an examination of patients with diabetic retinopathy and not RVO, these observations were consistent with the present findings in RVO-MAs.

Recently, Nakao et al qualitatively evaluated the diabetic MAs using confocal AOSLO and OCTA and suggested differences in the intra-aneurysmal blood flow at each MA [36]. In this study, using offset pinhole AOSLO, we could quantitatively evaluate the intra-aneurysmal BCM, which were found to be diverse at each MA type. The BCM index was 1.38 ± 0.25 in the focal bulge group and 1.16 ± 0.31 in the non-focal bulge group; this difference was significant. In the focal bulge group, the BCM were uniformly more rapid and turbulent compared to those in the non-focal bulge (see Visualization 1). The BCM in the non-focal bulge MAs, especially the MA accompanying cap, were uneven in identical MAs and more stagnant near the cap (see Visualization 2 and Visualization 3). The BCM index was 1.15 ± 0.24 in the MAs with the cap and 1.34 ± 0.29 in those without the cap; this difference was significant (Table 3). In addition, the BCM were negatively correlated with the cap size (Table 3). These results suggested that cap formation can be associated with intra-aneurysmal hemodynamics. We speculated that the more common observation of cap formations in non-focal bulge MAs might be a kind of vessel remodeling, which would help buffering the intra-aneurysmal turbulence that was more commonly observed in the focal bulge MAs. In diabetic MAs, Bernabeu et al. estimated intra-aneurysmal hemodynamics by using computational fluid dynamics; the low share rate was found to be associated with clot location in the saccular MAs [17]. These finding might implicate intra-aneurysmal endothelial damage in diabetic retinopathy and support the association between the low BCM and significant vascular leakage, which was more commonly observed in the non-FB RVO-MAs considered by the present study.

The FA in this study showed that retinal vascular leak was significantly associated with the morphology of the non-focal bulge, the formation and size of the cap, and lower BCM (Fig. 3, 5 and Table 4). The whole and lumen areas of the MAs were not significantly different between the MAs with and without dye leakage (Table 4). Wang et al examined diabetic MAs using FA and OCT, and showed results similar to ours, in which the MA size did not always correlate with the degree of dye leakage [37]. Since fluorescein leakage resulted from the dysfunction of the inner blood-retinal barrier made by tight junctions of the endothelial cells, the circumferential dilation of the fusiform MAs, the larger body of the saccular MA, or cap formation, it might indicate that the vessels associated with these non-focal MAs would have substantial endothelial damage. In this study, the calibers of the associated vessels were 12.0 ± 3.0 µm in the focal bulge MAs and 14.4 ± 3.0 µm in the non-focal bulge MAs (Table 2), which appeared to be greater than those of the physiological retinal capillaries of about 5-10 µm diameter [38, 39]. This indicated that the associated vessels of the non-focal bulge MA might be more congestive and the endothelial cells might be more vulnerable than those of the focal bulge MAs. However, an association between cap structure and vascular leakage is controversial. Circumferential and complete formations of the cap would rather contribute to the decrease in vascular leakage.

Our study has several limitations that should be considered when interpreting its findings. First, the sample size was small. Second, we examined several MAs in identical patients; therefore, we could not study the effects of the systemic factors. Third, the frames per second of our prototype offset pinhole AOSLO (30 frames per second) might not capture fast blood flow. However, the blood flow in MAs or in adjacent capillaries was slower than that in retinal arteries. Therefore, we considered that the AOSLO videos enabled the tracking of time-lapse motions of the blood cells (mainly erythrocytes) in the MAs. Fourth, the quantified BCM index may not strictly reflect the flow (velocity) of each RBC. Because of the disc shape of the RBCs, the indices can change depending on the angle between the measurement light of AOSLO and the RBC plane. Further, the hematocrits may affect image variance. The BCM index corresponds to the image variance at

the evaluated area and might, therefore, depend on the hemodynamic factors, such as the angles between RBC and the measuring light, hematocrits, and movement (flow). Lastly, we could not know the longitudinal change of each MA because this was a cross-sectional study.

However, the offset pinhole AOSLO visualized the ultrastructure and dynamics of the blood cells of the RVO-MAs, the characterizations of which are suggested to be associated with retinal vascular leakage. Longitudinal observation with AOSLO or basic research using immunohistochemistry is needed to confirm the results of our study and to deepen the understanding of the RVO-ME, or to establish new therapies.

5.   Conclusions

In this study, we used offset pinhole AOSLO for real-time imaging of the MA associated with RVO and examined the detail of the microstructure and intra-aneurysmal hemodynamics of blood cells. We found that the configurations of the MA were diverse, and some of them occasionally accompanied cap structure on the aneurysmal surface. Additionally, the morphologic and hemodynamic changes were significantly associated with fluorescein leakage.

Disclosures

The authors declare no conflicts of interest.

References

1. S. L. Rogers, R. L. McIntosh, L. Lim, P. Mitchell, N. Cheung, J. W. Kowalski, H. P. Nguyen, J. J. Wang, and T. Y. Wong, "Natural history of branch retinal vein occlusion: an evidence-based systematic review," Ophthalmology **117**(6), 1094–1101.e5 (2010).
2. S. S. Hayreh and M. B. Zimmerman, "Branch retinal vein occlusion: natural history of visual outcome," JAMA Ophthalmol. **132**(1), 13–22 (2014).
3. S. S. Hayreh, P. A. Podhajsky, and M. B. Zimmerman, "Natural history of visual outcome in central retinal vein occlusion," Ophthalmology **118**(1), 119–133.e2 (2011).
4. D. Finkelstein, "Argon laser photocoagulation for macular edema in branch vein occlusion," Ophthalmology **93**(7), 975–977 (1986).
5. P. A. Campochiaro, J. S. Heier, L. Feiner, S. Gray, N. Saroj, A. C. Rundle, W. Y. Murahashi, R. G. Rubio, and B. Investigators, "Ranibizumab for macular edema following branch retinal vein occlusion: six-month primary end point results of a phase III study," Ophthalmology **117**(6), 1102–1112.e1 (2010).
6. P. A. Campochiaro, W. L. Clark, D. S. Boyer, J. S. Heier, D. M. Brown, R. Vitti, H. Kazmi, A. J. Berliner, K. Erickson, K. W. Chu, Y. Soo, Y. Cheng, and J. A. Haller, "Intravitreal aflibercept for macular edema following branch retinal vein occlusion: the 24-week results of the VIBRANT study," Ophthalmology **122**(3), 538–544 (2015).
7. D. M. Brown, P. A. Campochiaro, R. P. Singh, Z. Li, S. Gray, N. Saroj, A. C. Rundle, R. G. Rubio, W. Y. Murahashi, and C. Investigators, "Ranibizumab for macular edema following central retinal vein occlusion: six-month primary end point results of a phase III study," Ophthalmology **117**(6), 1124–1133.e1 (2010).
8. J. F. Korobelnik, F. G. Holz, J. Roider, Y. Ogura, C. Simader, U. Schmidt-Erfurth, K. Lorenz, M. Honda, R. Vitti, A. J. Berliner, F. Hiemeyer, B. Stemper, O. Zeitz, R. Sandbrink, and G. S. Group, "Intravitreal Aflibercept Injection for Macular Edema Resulting from Central Retinal Vein Occlusion: One-Year Results of the Phase 3 GALILEO Study," Ophthalmology **121**(1), 202–208 (2014).
9. T. Horii, T. Murakami, K. Nishijima, A. Sakamoto, M. Ota, and N. Yoshimura, "Optical coherence tomographic characteristics of microaneurysms in diabetic retinopathy," Am. J. Ophthalmol. **150**(6), 840–848.e1 (2010).
10. M. Parravano, D. De Geronimo, F. Scarinci, L. Querques, G. Virgili, J. M. Simonett, M. Varano, F. Bandello, and G. Querques, "Diabetic Microaneurysms Internal Reflectivity on Spectral-Domain Optical Coherence Tomography and Optical Coherence Tomography Angiography Detection," Am. J. Ophthalmol. **179**, 90–96 (2017).
11. M. Parravano, D. De Geronimo, F. Scarinci, G. Virgili, L. Querques, M. Varano, F. Bandello, and G. Querques, "Progression of diabetic microaneurysms according to the internal reflectivity on structural optical coherence tomography and visibility on optical coherence tomography angiography," Am. J. Ophthalmol. **198**, 8–16 (2019).
12. H. W. Babcock, "Adaptive optics revisited," Science **249**(4966), 253–257 (1990).
13. A. Roorda and D. R. Williams, "The arrangement of the three cone classes in the living human eye," Nature **397**(6719), 520–522 (1999).
14. S. Ooto, M. Hangai, K. Takayama, A. Sakamoto, A. Tsujikawa, S. Oshima, T. Inoue, and N. Yoshimura, "High-resolution imaging of the photoreceptor layer in epiretinal membrane using adaptive optics scanning laser ophthalmoscopy," Ophthalmology **118**(5), 873–881 (2011).

15. K. Takayama, S. Ooto, M. Hangai, N. Ueda-Arakawa, S. Yoshida, T. Akagi, H. O. Ikeda, A. Nonaka, M. Hanebuchi, T. Inoue, and N. Yoshimura, "High-resolution imaging of retinal nerve fiber bundles in glaucoma using adaptive optics scanning laser ophthalmoscopy," Am. J. Ophthalmol. **155**(5), 870–881.e3 (2013).

16. J. Lammer, S. G. Karst, M. M. Lin, M. Cheney, P. S. Silva, S. A. Burns, L. P. Aiello, and J. K. Sun, "Association of Microaneurysms on Adaptive Optics Scanning Laser Ophthalmoscopy With Surrounding Neuroretinal Pathology and Visual Function in Diabetes," Invest. Ophthalmol. Visual Sci. **59**(13), 5633–5640 (2018).

17. M. O. Bernabeu, Y. Lu, O. Abu-Qamar, L. P. Aiello, and J. K. Sun, "Estimation of Diabetic Retinal Microaneurysm Perfusion Parameters Based on Computational Fluid Dynamics Modeling of Adaptive Optics Scanning Laser Ophthalmoscopy," Front Physiol **9**, 989 (2018).

18. S. G. Karst, M. Salas, J. Hafner, C. Scholda, W. D. Vogl, W. Drexler, M. Pircher, and U. Schmidt-Erfurth, "Three-Dimensional Analysis of Retinal Microaneurysms with Adaptive Optics Optical Coherence Tomography," Retina **39**(3), 465–472 (2019).

19. T. Y. Chui, T. J. Gast, and S. A. Burns, "Imaging of vascular wall fine structure in the human retina using adaptive optics scanning laser ophthalmoscopy," Invest. Ophthalmol. Visual Sci. **54**(10), 7115–7124 (2013).

20. T. Y. Chui, M. Dubow, A. Pinhas, N. Shah, A. Gan, R. Weitz, Y. N. Sulai, A. Dubra, and R. B. Rosen, "Comparison of adaptive optics scanning light ophthalmoscopic fluorescein angiography and offset pinhole imaging," Biomed. Opt. Express **5**(4), 1173–1189 (2014).

21. T. Y. Chui, D. A. Vannasdale, and S. A. Burns, "The use of forward scatter to improve retinal vascular imaging with an adaptive optics scanning laser ophthalmoscope," Biomed. Opt. Express **3**(10), 2537–2549 (2012).

22. "Classification of diabetic retinopathy from fluorescein angiograms. ETDRS report number 11. Early Treatment Diabetic Retinopathy Study Research Group," *Ophthalmology* 98, 807–822 (1991).

23. V. Schreur, A. Domanian, B. Liefers, F. G. Venhuizen, B. J. Klevering, C. B. Hoyng, E. K. de Jong, and T. Theelen, "Morphological and topographical appearance of microaneurysms on optical coherence tomography angiography," Br J Ophthalmol **103**(5), 630–635 (2019).

24. A. Uji, M. Hangai, S. Ooto, K. Takayama, N. Arakawa, H. Imamura, K. Nozato, and N. Yoshimura, "The source of moving particles in parafoveal capillaries detected by adaptive optics scanning laser ophthalmoscopy," Invest. Ophthalmol. Visual Sci. **53**(1), 171–178 (2012).

25. S. Arichika, A. Uji, M. Hangai, S. Ooto, and N. Yoshimura, "Noninvasive and direct monitoring of erythrocyte aggregates in human retinal microvasculature using adaptive optics scanning laser ophthalmoscopy," Invest. Ophthalmol. Visual Sci. **54**(6), 4394–4402 (2013).

26. T. Y. Chui, Z. Zhong, H. Song, and S. A. Burns, "Foveal avascular zone and its relationship to foveal pit shape," Optom Vis Sci **89**(5), 602–610 (2012).

27. J. Moore, S. Bagley, G. Ireland, D. McLeod, and M. E. Boulton, "Three dimensional analysis of microaneurysms in the human diabetic retina," J. Anat. **194** (1), 89–100 (1999).

28. A. W. Stitt, T. A. Gardiner, and D. B. Archer, "Histological and ultrastructural investigation of retinal microaneurysm development in diabetic patients," Br. J. Ophthalmol. **79**(4), 362–367 (1995).

29. M. Dubow, A. Pinhas, N. Shah, R. F. Cooper, A. Gan, R. C. Gentile, V. Hendrix, Y. N. Sulai, J. Carroll, T. Y. Chui, J. B. Walsh, R. Weitz, A. Dubra, and R. B. Rosen, "Classification of human retinal microaneurysms using adaptive optics scanning light ophthalmoscope fluorescein angiography," Invest. Ophthalmol. Visual Sci. **55**(3), 1299–1309 (2014).

30. A. G. Bennett, A. R. Rudnicka, and D. F. Edgar, "Improvements on Littmann's method of determining the size of retinal features by fundus photography," Graefe's Arch. Clin. Exp. Ophthalmol. **232**(6), 361–367 (1994).

31. P. E. DiCorleto, C. M. Gajdusek, S. M. Schwartz, and R. Ross, "Biochemical properties of the endothelium-derived growth factor: comparison to other growth factors," J. Cell. Physiol. **114**(3), 339–345 (1983).

32. G. Rath, C. Dessy, and O. Feron, "Caveolae, caveolin and control of vascular tone: nitric oxide (NO) and endothelium derived hyperpolarizing factor (EDHF) regulation," *J Physiol Pharmacol* 60 Suppl 4, 105–109 (2009).

33. K. Yamamoto, T. Takahashi, T. Asahara, N. Ohura, T. Sokabe, A. Kamiya, and J. Ando, "Proliferation, differentiation, and tube formation by endothelial progenitor cells in response to shear stress," J. Appl. Physiol. **95**(5), 2081–2088 (2003).

34. A. Ishibazawa, T. Nagaoka, T. Takahashi, K. Yamamoto, A. Kamiya, J. Ando, and A. Yoshida, "Effects of shear stress on the gene expressions of endothelial nitric oxide synthase, endothelin-1, and thrombomodulin in human retinal microvascular endothelial cells," Invest. Ophthalmol. Visual Sci. **52**(11), 8496–8504 (2011).

35. J. Frosen, J. Cebral, A. M. Robertson, and T. Aoki, "Flow-induced, inflammation-mediated arterial wall remodeling in the formation and progression of intracranial aneurysms," Neurosurg Focus **47**(1), E21 (2019).

36. S. Nakao, S. Yoshida, Y. Kaizu, M. Yamaguchi, I. Wada, T. Ishibashi, and K. H. Sonoda, "Microaneurysm Detection in Diabetic Retinopathy Using OCT Angiography May Depend on Intramicroaneurysmal Turbulence," Ophthalmol Retina **2**(11), 1171–1173 (2018).

37. H. Wang, J. Chhablani, W. R. Freeman, C. K. Chan, I. Kozak, D. U. Bartsch, and L. Cheng, "Characterization of diabetic microaneurysms by simultaneous fluorescein angiography and spectral-domain optical coherence tomography," Am. J. Ophthalmol. **153**(5), 867 (2012).

38. M. Hogan, J. Alvarado, and J. Weddell, *Histology of the Human Eye: An Atlas and Textbook* (B Saunders Co, 1971), 515–519 .

39. Q. Wang, O. P. Kocaoglu, B. Cense, J. Bruestle, R. S. Jonnal, W. Gao, and D. T. Miller, "Imaging retinal capillaries using ultrahigh-resolution optical coherence tomography and adaptive optics," Invest. Ophthalmol. Visual Sci. **52**(9), 6292–6299 (2011).